Journal of
Mechanics of
Materials and Structures

SHAFT-HUB PRESS FIT SUBJECTED TO COUPLES AND RADIAL FORCES: ANALYTICAL EVALUATION OF THE SHAFT-HUB DETACHMENT LOADING

Enrico Bertocchi, Luca Lanzoni, Sara Mantovani, Enrico Radi and Antonio Strozzi

Volume 13, No. 3 May 2018

msp

JOURNAL OF MECHANICS OF MATERIALS AND STRUCTURES
Vol. 13, No. 3, 2018
dx.doi.org/10.2140/jomms.2018.13.283

SHAFT-HUB PRESS FIT SUBJECTED TO COUPLES AND RADIAL FORCES: ANALYTICAL EVALUATION OF THE SHAFT-HUB DETACHMENT LOADING

ENRICO BERTOCCHI, LUCA LANZONI, SARA MANTOVANI, ENRICO RADI AND ANTONIO STROZZI

A shaft-hub press fit subjected to two non-axisymmetric loading conditions is examined and the situation of incipient detachment between the shaft and the hub is determined. The first condition consists of a central radial load P applied to the hub, balanced by two lateral forces $P/2$ applied to the shaft at a distance d from the hub lateral walls. In the second condition, a central couple C is applied to the hub, and it is balanced by two lateral opposite loads withstood by the shaft at a distance d from the hub lateral walls. The shaft-hub contact is modelled in terms of two elastic Timoshenko beams connected by distributed elastic springs (Winkler foundation), whose constant is analytically evaluated. Based upon this enhanced beam-like modelling, the loading inducing an undesired shaft-hub incipient detachment is theoretically determined in terms of the shaft-hub geometry, of the initial shaft-hub interference, and of the elastic constants. Finite element forecasts are presented to quantify the error of this beam-like approximate analytical approach.

1. Introduction

Press fit between a hub and a shaft is a widely employed clamping method, but it can lead to problems of fretting fatigue if the clamping pressure generated by interference is insufficient to prevent slip. A limit situation in which slip inevitably occurs is when the loading applied to the shaft-hub assembly causes an appreciable shaft bending that in turn produces incipient detachment between the shaft and the hub. This incipient detachment situation is an indicator of poor mechanical design, and it may be assumed as a reference condition against the outcome of fretting.

The title problem bears some similarity with the press fit of the bush into a connecting rod small end [Marmorini et al. 2012]. The undesired event is bush loosening, since it favours bush rotation, which would occlude the lubrication hole; the load that produces bush loosening is assumed as a reference loading, and the admissible force must exhibit a safety factor with respect to the reference load threshold.

The available models of the shaft-hub press fit possess an extensive literature spread over various decades, which may be classified into three main groups. The first category collects the classical, axisymmetric, plane solution of a shaft-hub interference fit. This solution neglects the possible outcome of pressure peaks at the contact extremities, and it ignores loadings that produce shaft bending. The second group addresses the evaluation, for an axisymmetric loading, of the pressure bumps occurring at the contact extremities. The third set considers both the presence of lateral pressure peaks and of shaft bending, caused by a non axisymmetric loading. Extended literature review on these three topics is available in [Strozzi et al. 2011; 2016; Croccolo et al. 2012; Smetana 2001; Radi et al. 2017].

Keywords: press fit, incipient detachment, analytical solution, Winkler foundation, finite elements.

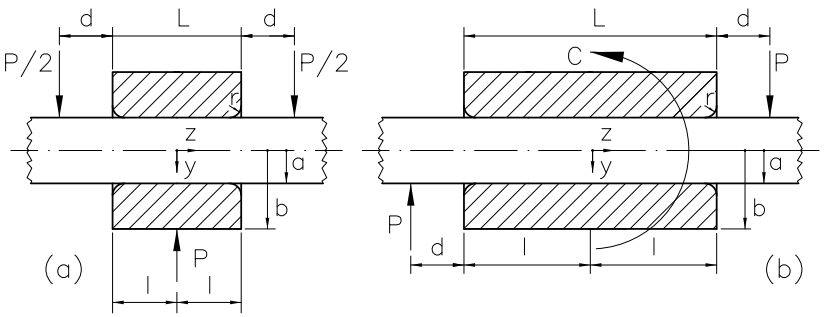

Figure 1. The two loading conditions (a) and (b) in terms of the forces P and the couple C, and the meaning of the symbols a, b, d, l, L, r, y, z.

This paper presents both analytical and numerical investigations on the mechanical response of a shaft-hub press fit subjected to an external, non axisymmetric loading. Two loading conditions of practical interest are addressed:

(i) A central radial load P is sustained by the hub, and it is equilibrated by two lateral forces $P/2$ applied to the shaft at a distance d from the hub lateral walls (Figure 1a).

(ii) A central couple C applied to the hub is equilibrated by two lateral loads $P = C/[2(l+d)]$, sustained by the shaft at a distance d from the hub lateral walls (the hub length being L), and having opposite directions (Figure 1b).

Figure 1 also clarifies the meaning of the symbols a, b, d, l, L, r, y, z.

This practically oriented paper complements a previous work addressing a press-fit, in which the shaft was deflected by two equal bending couples applied to the shaft extremities [Strozzi et al. 2016; Radi et al. 2017]. The above loading together with the two additional loadings illustrated in Figure 1 constitute three loading conditions considered in the DIN standards discussed in the two papers cited.

The main aim of this paper is to determine the intensity of the bending loading that locally annihilates the initial contact pressure due to the shaft-hub press fit alone, and it begins the detachment between the shaft and the hub. As already noted, the occurrence of a shaft-hub separation constitutes an indicator of poor mechanical design, since it promotes undesired phenomena of wear and fretting fatigue [Ciavarella et al. 1998]. Such observations justify this return to the analysis of situations of incipient detachment.

A rigorous three-dimensional analytical modelling of the detachment condition being prohibitively complex, the modelling of the shaft-hub contact is approximated in terms of two elastic Timoshenko beams connected by distributed elastic springs (Winkler model), see [Radi et al. 2017]; the classical Lamé solution is employed to simulate the press-fit stresses in the absence of external loading. The analytical evaluation of the intensity of the loading that locally begins the detachment between the shaft and the hub is achieved by separately evaluating the frictionless contact pressure due to the press-fit alone, and the contact pressure imputable to the shaft bending alone. The corresponding solutions are briefly considered in the following sections; further details can be found in [Radi et al. 2017].

The authors are aware of the availability of alternative approaches for describing the incipient detachment between two bodies; see, e.g., [Deseri and Owen 2003; 2010]. However, the two-beam model already employed in [Radi et al. 2017] was found to be suitable for our purposes.

The analytical prediction of the detachment loading when the shaft is loaded by couples at its extremities, presented in [Radi et al. 2017], indicates that the unavoidably approximate beam-like modelling favoured in this paper to describe this contact detachment problem supplies an indicative value rather than an accurate threshold of the critical loading. It is therefore expected that for the two loading conditions illustrated in Figure 1 the analytical solution be approximate, although still technically significant. Various three-dimensional finite element (FE) forecasts are included in this paper, that provide an accurate prediction of the detachment loading, albeit only for a selection of press-fit geometries, and they permit the evaluation of the error incurred in the approximate analytical approach.

The FE forecasts of [Strozzi et al. 2016] indicate that, if the hub bore edges are rounded, the couple that produces the shaft-hub detachment is higher than its counterpart valid for sharp hub bore edges. In practical situations, this increase may be of, say, 20 per cent. A thorough modelling of the shaft-hub detachment problem should therefore incorporate the hub bore fillet radius effect. However, since the main aim of this paper is to determine an indicative value of the detachment loading rather than its accurate threshold, the effect of the hub bore rounded edges is not explored in this paper, and reference is made to a sharp bore edge both in the analytical and in the FE studies.

In [Radi et al. 2017] the press fits subjected to bending have been classified into two main categories. The first group collects problems in which the shaft laterally protrudes from both the hub sides, and the shaft projecting portions are subjected to bending, as in the two couplings of Figure 1. Bearing mounting often belongs to this category. The second group embraces situations where the shaft protrudes from only one side of the hub, whereas the remaining shaft extremity is aligned with one of the two hub lateral faces; in this case, the external loading is applied to the shaft protrusion and to the hub. The crankpin press-fitting into a crankweb in a composite crankshaft [Smetana 2001; Strozzi and Vaccari 2003] belongs to this second group. This paper addresses the first category by examining in detail two detachment problems whose geometries and loadings are illustrated in Figure 1, and it is organized as follows. Section 2 considers the contact pressure due to press fit alone, whereas Section 3 addresses the contact pressure caused by the shaft bending alone; Section 4 analytically evaluates the Winkler constant; Section 5 imposes the incipient detachment condition; Section 6 reports fundamental solutions in the FE study; Section 7 compares analytical and FE forecasts.

2. Press-fit contact pressure

The shaft-hub contact pressure due to the press-fit alone is axisymmetric, and it stays reasonably constant in its central part, whereas it exhibits localized pressure bumps at the shaft-hub contact extremities, where the hub bore edges are rounded. Overall, the pressure profile is camel backed [Strozzi et al. 2011; Croccolo et al. 2012]. The analytical value of the elastic flattish central contact pressure p_{pf} (the index pf denotes "press fit") is correctly forecast by the Lamé plane modelling, e.g. [Strozzi et al. 2011]:

$$p_{\mathrm{pf}} = \frac{E\delta}{2a}(1-\alpha^2), \tag{1}$$

where a denotes the nominal value of both the shaft radius (the shaft is assumed to be solid) and of the hub inner radius, $\alpha = a/b$, and b represents the hub outer radius, Figure 1. In addition, δ denotes the radial interference, and E is the Young's modulus of the material of both the above components.

No simple expression is available that quantifies the lateral pressure bumps [Strozzi et al. 2011; Croccolo et al. 2012]. Since the shaft detaches from the hub starting from their contact extremities, at a first sight the detachment loading is expected to be appreciably influenced by such pressure bumps, whose presence cannot therefore be ignored. However, since the pressure bumps are extremely localized, when the loading produces an axial extent of the shaft-hub detachment higher than that of the pressure bump, the pressure bumps disappear, and the contact pressure smoothly decays from its flattish central value to zero [Strozzi et al. 2016]. It may therefore be concluded that, when computing the loading that initiates the shaft-hub separation, it is acceptable to refer to the flattish central contact pressure of formula (1) and to neglect the lateral pressure bumps; see [Strozzi et al. 2016] for additional details.

3. Contact pressure due to the shaft bending

This section addresses the analytical evaluation of the frictionless contact pressure bilaterally exerted between the shaft and the hub in the presence of a perfect fit, i.e., in the absence of interference or clearance, as a result of the external loading alone, see Figure 1. The shaft-hub contact is assumed as bilateral, since this paper addresses and incipient detachment condition rather than a partially detached contact. Following [Radi et al. 2017], the shaft and the hub are described in terms of two Timoshenko beams according to a shear-deformable modelling, endowed with a Winker foundation to account for the deformations of the shaft and hub cross sections due to the in-plane stresses. The analytical approach follows the same lines as those detailed in [Radi et al. 2017] for the shaft loading constituted by two couples, to which the interested reader is referred; attention is paid in Sections 3.1 and 3.2 to the boundary conditions to be applied to the two beams for the two loadings detailed in Figure 1, whereas only a perfunctory description of the analytical solution of the two contact problems of Figure 1 is reported in this paper.

The governing equation of this beam contact problem is the fourth order ODE [Radi et al. 2017]:

$$\frac{d^4\Phi}{dz^4} - \frac{4\varepsilon\lambda^2}{l^2}\frac{d^2\Phi}{dz^2} + \frac{4\lambda^4}{l^4}\Phi = 0, \tag{2}$$

where the non-dimensional constants λ and ε have been introduced together with the auxiliary constant γ:

$$\lambda^4 = \frac{Kl^4}{4}\Big(\frac{1}{EI_1} + \frac{1}{EI_0}\Big), \quad \gamma^2 = \frac{Kl^2}{4}\Big(\frac{\chi_1}{GA_1} + \frac{\chi_0}{GA_0}\Big). \tag{3}$$

$$\varepsilon = \frac{\gamma^2}{\lambda^2} = \Big(\frac{\chi_1}{GA_1} + \frac{\chi_0}{GA_0}\Big)\sqrt{\frac{KEI_0I_1}{4(I_0+I_1)}} = \frac{1+\nu}{2}\sqrt{\frac{K}{\pi E}\frac{1+\alpha^2}{1-\alpha^2}}\,\big[(1-\alpha^2)\chi_1 + \alpha^2\chi_0\big]. \tag{4}$$

In (2), Φ denotes the relative rotation between two cross sections of the two beams describing the shaft and the hub, respectively, at the same axial coordinate z, Figure 1, and l is the hub half length. In addition, K is the Winkler constant, E is the Young's modulus, G is the shear modulus, A_0 and A_1 are the areas of the cross sections of the two beams, I_0 and I_1 are their moments of inertia, and χ_0 and χ_1 are their shear factors, see [Radi et al. 2017], respectively. A discussion on the evaluation of the Winkler constant K is postponed to Section 4.

The general solution of the ODE (2) in terms of Φ is:

$$\begin{aligned}\Phi(z) = &\left[c_1 \sin\left(\lambda\sqrt{1-\varepsilon}\,\frac{z}{l}\right) + c_2 \cos\left(\lambda\sqrt{1-\varepsilon}\,\frac{z}{l}\right)\right]\cosh\left(\lambda\sqrt{1+\varepsilon}\,\frac{z}{l}\right)\\ &+\left[c_3 \sin\left(\lambda\sqrt{1-\varepsilon}\,\frac{z}{l}\right) + c_4 \cos\left(\lambda\sqrt{1-\varepsilon}\,\frac{z}{l}\right)\right]\sinh\left(\lambda\sqrt{1+\varepsilon}\,\frac{z}{l}\right),\end{aligned} \tag{5}$$

where c_i $(i = 1, 2, 3, 4)$ are non-dimensional constants to be determined by imposing the boundary conditions at $z = 0, l$.

The contact force q between the two beams is obtained by repeatedly differentiating Φ according to formula (6) [Strozzi et al. 2016]. Since it has been ascertained that, for the cases examined, the shaft-hub separation always initiates from the hub extremities defined by $z = l$ [Radi et al. 2017], and not at the hub centre, it is important to evaluate therein the value of the contact force q. Finally, the corresponding maximum contact pressure $p_{\max}$ has been estimated in formula (6) by assuming a cosinusoidal distribution of the contact pressure in the circumferential direction; see [Radi et al. 2017] for additional details:

$$q = K\frac{l^4}{4\lambda^4}\frac{d^3\Phi}{dz^3}, \quad q(l) = \frac{Kl^4}{4\lambda^4}\frac{d^3\Phi(l)}{dz^3}, \quad p_{\max} = \frac{Kl^4}{4\pi r_i \lambda^4}\frac{d^3\Phi(l)}{dz^3}. \tag{6}$$

The boundary conditions for the two loadings of Figures Figure 1a and 1b are separately treated in Sections 3.1 and 3.2.

3.1. ***Boundary conditions for the loading constituted by a central force and by two lateral equilibrating forces.*** In this Section the loading condition is examined in which a central radial force P applied to the hub is equilibrated by two lateral forces $P/2$ applied to the shaft at a distance d from the hub lateral walls, Figure 1a. The aim of this Section is to formulate the corresponding boundary conditions for the beam modelling.

It is convenient to refer to the statically equivalent loading detailed in Figure 2, in which the two forces $P/2$ applied to the shaft at a distance d from the hub lateral walls, Figure 1a, are substituted by two forces $P/2$ applied to the shaft section aligned with the hub lateral walls, and by two couples $C = Pd/2$ applied to the shaft. Figure 2 also clarifies the origin of the z coordinate.

The four unknown constants c_i of the general solution expressed by (5) are evaluated by imposing four boundary conditions, expressing that a) at the shaft-hub contact midpoint, i.e., for $z = 0$, the unknown function Φ vanishes, whereas the shear force assumes the value $P/2$, consistent with the presence of the central force P applied to the hub, and that b) at the shaft-hub contact extremity, i.e. for $z = l$, the

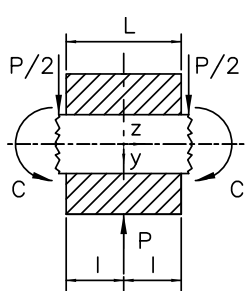

Figure 2. The boundary conditions to be applied to the beam for the loading of Figure 1a.

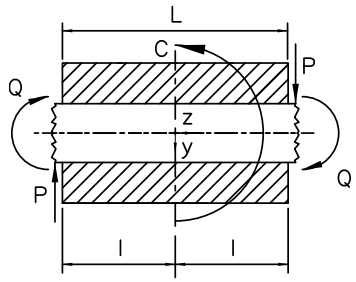

Figure 3. The boundary conditions to be applied to the beam and to the hub for the loading of Figure 1b.

bending moment M_{i} and the shear force T_{i} (indices 0 and 1 denote the hub and the shaft, respectively) equal the applied moment $C = Pd/2$ and the force P, within the respect of the sign conventions of Figure 4 of [Radi et al. 2017]:

$$\Phi(0) = 0, \quad \frac{d^2\Phi}{dz^2}(0^+) = -\frac{P}{2EI_0}, \quad \frac{d\Phi}{dz}(l) = -\frac{C}{EI_1} = -\frac{Pd}{2EI_1}, \quad \frac{d^2\Phi}{dz^2}(l) = \frac{P}{2EI_1}. \tag{7}$$

The expressions of the four unknown constants c_i are too long to be reported here.

3.2. ***Boundary conditions for the loading constituted by a central couple and by two lateral equilibrating forces of opposite directions.*** In this section the loading condition is examined in which a central couple applied to the hub is balanced by two lateral, opposite forces $P = C/[2(l+d)]$ exerted on the shaft at a distance d from the hub lateral walls, Figure 1b. The aim of this Section is to formulate the corresponding boundary conditions for the beam modelling.

It is advantageous to refer to the statically equivalent loading detailed in Figure 3, in which the two forces P applied to the shaft at a distance d from the hub lateral walls are substituted by two forces P exerted on the shaft section aligned with the hub lateral walls, and by two couples $Q = Pd$ withstood by the shaft.

The four unknown constants c_{i} of (5) are evaluated by imposing four boundary conditions, expressing that a) at the shaft-hub contact midpoint, i.e., for $z = 0$, the loading is skew-symmetric, and, therefore, the bending moment assumes the value reported in (8), whereas the contact force q is null, thus implying that $\mathrm{d}^3/\mathrm{d}z^3 = 0$ according to (6); b) the shear force and the bending moment at the shaft-hub contact extremity, i.e. for $z = l$, assume the values reported in (8), within the respect of the sign conventions of Figure 4 of [Radi et al. 2017]:

$$\frac{d\Phi}{dz}(0^+) = \frac{C}{2EI_0}, \quad \frac{d^3\Phi}{dz^3}(0) = 0, \quad \frac{d\Phi}{dz}(l) = -\frac{Cd}{[2(l+d)]EI_1}, \quad \frac{d^2\Phi}{dz^2}(l) = \frac{C}{[2(l+d)]EI_1}. \tag{8}$$

4. Evaluation of the Winkler constant

It has been observed in [Radi et al. 2017] that the introduction of a Winkler model in the analytical description of the contact interaction between the shaft and the hub is physically advantageous, since it avoids the outcome of stress singularities at the contact extremities.

In [Radi et al. 2017] various models proposed for evaluating the Winkler constant have been compared, and it has been shown that its numerical value noticeably varies according to the approach employed. In particular, in formula (12) of [Lundberg 1958] the deformability of the shaft-hub cross section has been estimated by adopting a plane model formed by a hollow disk surrounded by a ring, and by adopting a simplified loading. A closed form expression has been obtained for the Winkler constant K:

$$\frac{K}{2G} = \frac{\pi(1+\nu)}{(1-\nu)}\left[1+\left(\frac{a_{\mathrm{i}}}{a}\right)^2\right]\left[1+\left(\frac{a}{b}\right)^2\right]\left[1-\left(\frac{a_{\mathrm{i}}}{a}\right)^2\left(\frac{a}{b}\right)^2\right]^{-1}, \tag{9}$$

where a_{i}, a, and b are the inner, intermediate, and outer radii, respectively. For $\nu = 0.3$, for a solid shaft ($a_{\mathrm{i}} = 0$), and for the reference configuration $b = 2a$, $K/(2G) = 7.29$.

The radial compliance of a solid circular cross section surrounded by a ring is analytically examined in [Strozzi et al. 2016]. Following the approach of [Castillo and Barber 1997], the differences between the shear stresses acting on the two plane cross sections of a thin shaft slice are replaced by body forces. The exact distribution of the shear stresses τ_{rz} and $\tau_{\theta\mathrm{z}}$ due to a shear force is analytically available both for a solid disk and a ring, [Love 1944, p. 335]. The analytical expression of the Winkler constant has been evaluated in [Radi et al. 2017] with an energy approach based on the Clapeyron theorem. Within this model, for the above reference geometry $\alpha = a/b = 1/2$ and for $\nu = 0.3$ and adopting plane strain, the normalized Winkler constant $K/(2G)$ is 1.90.

An alternative model for evaluating the Winkler constant assumes that the body forces representative of the shear stresses be uniformly distributed according to a gravitational field within both the solid disk and the ring, see Figure 2a of [Castillo and Barber 1997]. In this case, the analytical solution provides $K/(2G) = 3.68$ for $\alpha = a/b = 1/2$ and for $\nu = 0.3$ in plane strain.

In the present work we propose an alternative procedure for evaluating the Winkler constant, based on the virtual work theorem. We assume indeed a uniform distribution of shear stress, whose resultants are a unit shear force in the shaft and an opposite unit shear force in the hub, as the virtual stress field working for the actual distribution of shear strain provided in [Radi et al. 2017] as τ_{rz}/G and $\tau_{\theta\mathrm{z}}/G$ and due to the opposite shear forces Q acting on shaft and hub. The latter work is then compared to that carried out by the unit shear forces acting on shaft and hub for the actual relative displacement between shaft and hub, namely Q/K. In this case, the analytical expression of $K/(2G)$ becomes:

$$\frac{K}{2G} = \frac{48\pi}{D}(1-\alpha^4)^2(1-\nu^2), \tag{10}$$

where

$$D = \big\{(1-\alpha^2)[15-33\nu-20\nu^2+64\nu^3+\alpha^2(34-46\nu-72\nu^2+80\nu^3)+\alpha^4(35-77\nu-4\nu^2+48\nu^3)] \\ - 12(1+\alpha^2)[3-\nu-4\nu^2+2\alpha^2(3-\nu-2\nu^2)]\ln\alpha\big\}. \tag{11}$$

With this model, for $\alpha = a/b = 1/2$ and for $\nu = 0.3$, $K/(2G) = 2.6933$ under plane strain conditions.

The Winkler constant derived from the application of the principle of virtual work does not need to be strictly positive. In fact, for $\nu \cong -0.9$ the normalized Winkler constant exhibits an unphysical singular behavior. However, the press-fit problem examined in this paper deals with classical elastic materials whose Poisson's ratio is positive and, therefore, this anomaly has not been examined further.

Figure 4 reports the normalized Winkler constant $K/(2G)$ versus $\alpha = a/b$ for the three above models, i.e., for the body forces according to the exact shear stress distribution, referred to as "Love", for the

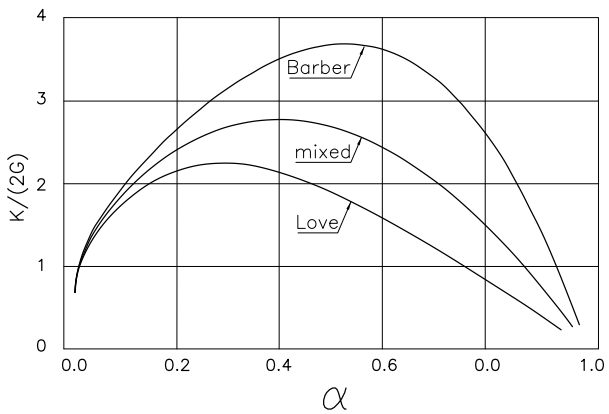

Figure 4. Three normalized Winkler constants $K/(2G)$ in terms of $\alpha = a/b$, for $\nu = 0.3$, in plane strain.

shear stresses distributed according to a gravitational loading, named "Barber", and for the proposed combination of the two above stress distributions, denoted "mixed". Plane strain is assumed, and $\nu = 0.3$. The corresponding values are reasonably comparable; the foundation of (9) supplies considerably higher values and, therefore, it has not been included in Figure 4. Note that the limit of $K/(2G)$ for $\alpha = 0, 1$ vanishes, according to its physical meaning.

In [Radi et al. 2017] it has been noted that, in the region where the shaft-hub separation begins, the shaft protrudes from the hub, so that the cross section of the shaft projecting part, being no longer directly compressed by the contact pressure, but being only deflected by the bending moment, remains reasonably undeformed with respect to its counterpart directly compressed by the hub. The above observation suggests that the Winkler constant may be more realistically evaluated by considering only the in-plane deformability of the hub cross section, whereas the deformability of the shaft cross section is neglected. This assumption produces an increase of the Winkler constant, albeit moderate. For $\alpha = a/b = 1/2$ and for $\nu = 0.3$ under plane strain conditions, the normalized Winkler constant increases to 2.31 for the "Love" model, to 4.81 for the "Barber" model, and to 3.39 for the "mixed" model. The above assumption for the evaluation of the Winkler constant has been adopted in this paper in the compilation of the detachment diagrams; see Figures 6 and 7.

5. Incipient detachment condition

The condition of shaft-hub incipient detachment requires that the contact pressure p_{if} due to the press fit alone and expressed by (1) equals the opposite of the maximum contact pressure $p_{\max}$ caused by the shaft bending alone, and expressed by (6):

$$p_{\mathrm{if}} = p_{\max} \Rightarrow \frac{E\delta}{2a}(1-\alpha^2) = -\frac{Kl^4}{4\pi r_{\mathrm{i}}\lambda^4}\frac{d^3\Phi(l)}{dz^3}. \tag{12}$$

Equation (12) allows the evaluation of the analytical value of the loading that initiates the shaft-hub detachment. For the loading of Figure 1a, Equation (12) supplies the critical value of the force P, whereas for the loading of Figure 1b it provides the critical value of the couple C.

6. Finite element study

The approximate beam-like modelling developed in this paper supplies an indicative, although still technically significant, value of the incipient detachment loading. To quantify the error incurred by the beam-like approach, various three-dimensional finite element (FE) forecasts have been presented in Section 7, that supply an accurate prediction of the detachment loading, albeit only for a selection of press-fit geometries.

The commercial FE program MSC Marc 2013 has been employed in this study. The 3D mesh is formed by about 23000 biquadratic quadrilateral elements adopting a Fourier formulation. The element size grades smoothly from 0.016 times the shaft radius a at the indenting edge, to 0.1 times in the zones far from the stress singularity. For all the test cases, a refined mesh with halved element sides was employed to assess the numerical convergence. The relative error of the coefficient H defining the radial stress singular term, see below, was found to be 0.14 per cent. A similar mesh is displayed in Figure 3 of [Strozzi et al. 2016].

The FE solutions for the two problems described in Figure 1 express the normalized detachment loading for the following three normalized geometries, namely a) the ratio a/b between the hub inner and outer radii; b) the ratio a/L between the shaft radius and the hub axial length; c) the ratio d/a of the distance of the lateral loadings from the hub lateral faces, to the shaft radius.

To limit the computational effort, fundamental FE loadcases have been identified in Figure 5, whose superposition provides the detachment loading for a general d/a value, although for prescribed values of a/b and a/L. Figure 5(a) addresses the frictionless stress field due to the interference alone, whereas the remaining Figs consider various loadings for a shaft-hub perfect fit, bilateral, frictionless contact pressure. For the loading of Figure 1(a), the three suitable fundamental loadcases are presented in Figures 5(a), 5(b), 5(c), whereas for the loading of Figure 1(b), the three fundamental loadcases are those of Figures 5(a), 5(d), 5(e).

For instance, suitable combinations of the loadings of Figures 5(b) and 5(c) allow various distances d of the lateral forces P from the hub sides to be modelled for a perfect fit. Consequently, for a prescribed d, the relative weights of the solutions of Figures 5(b) and 5(c) may be determined. The weight of the solution of Figure 5(a), supplying the shaft-hub press-fit stresses, may be evaluated by numerically imposing, similar to the analytical condition of Section 5, the incipient detachment condition through the vanishing of the contact pressure where detachment begins. In other words, the correct combination of the previous fundamental solutions must annihilate the radial stress at the sharp edge at the hub bore side.

Unfortunately, it is difficult to robustly implement the above procedure in a FE analysis. In fact, for a general loading, the sharp edge produces a theoretically unbounded contact pressure. To circumvent this numerical difficulty, an incipient detachment condition has been adopted that is based on the non-singular displacement field, see Appendix 4 of [Strozzi et al. 2015]. In more detail, according to the dominant term of the Williams asymptotic expansion, the stress tensor singularly behaves as $H \times f_{ij}(\varphi) \times s^{-0.226}$, whereas the displacement vector non singularly behaves as $H \times g_i(\varphi) \times s^{1-0.226}$, where (s, φ) is a local polar coordinate system along the meridional plane of Figure 1, whose origin falls at the sharp edge of the hub bore. The expressions of the f_{ij}, and g_{i} functions are known, and they are independent of the loading. In [Yosibash and Szabó 1995] it is shown that the singularity strength is the same for a plane

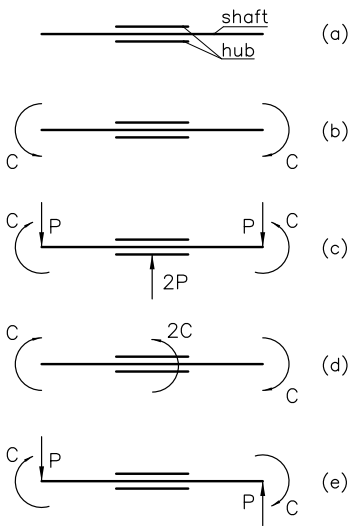

Figure 5. Five basic solutions.

and for an axisymmetric domain, see also [Huang and Leissa 2007]. The incipient detachment condition requires that σ_r vanishes at the sharp edge, which in turn demands that H too be null.

It is numerically convenient to compute H by sampling the FE radial displacement component moving along the hub lateral face, rather than the radial stress component moving along the contact interface. A best fitting procedure is then employed to extract the multiplying coefficient H of $u_r = H \times g_r(0) \times s^{1-0.226}$.

The coefficient H has been evaluated for all the loadcases of Figure 5. Returning to the above example, the relative weights of the two loadcases of Figure 5(b) and 5(c) may be determined by imposing the value of the distance d, Figure 1(a). Such weights depend on the external loading, on the coupling geometry, and on the Poisson ratio. The weight of the loadcase of Figure 5(a) depends on the initial interference, on the coupling geometry, on the Poisson ratio, and linearly on the Young's Modulus; it may be determined by imposing that the superposition of the three above loadcases produces a null coefficient H. It is concluded that this numerical procedure determines the relationship between the initial interference and the external loading, for a prescribed press-fit geometry and for given elastic constants.

7. Comparison between analytical and FE forecasts

As noted in the Introduction, the unavoidably approximate beam-like modelling of the two contact problems (a) and (b) of Figure 1 supplies the order of magnitude of the critical loading rather than an accurate forecast of its threshold. For this reason, various FE forecasts have been enclosed in this paper, that supply accurate predictions of the detachment loading, although only for selected press fit geometries, and they permit the error incurred by the simplified analytical approach to be quantified. The comparison between analytical and FE forecasts for the two press-fit loadings detailed in Figures 1(a) and 1(b) is separately presented in the following two Sections 7.1 and 7.2. As discussed in the Introduction, reference is made for simplicity to hub bore sharp edges, and the effect of a fillet radius is not explored.

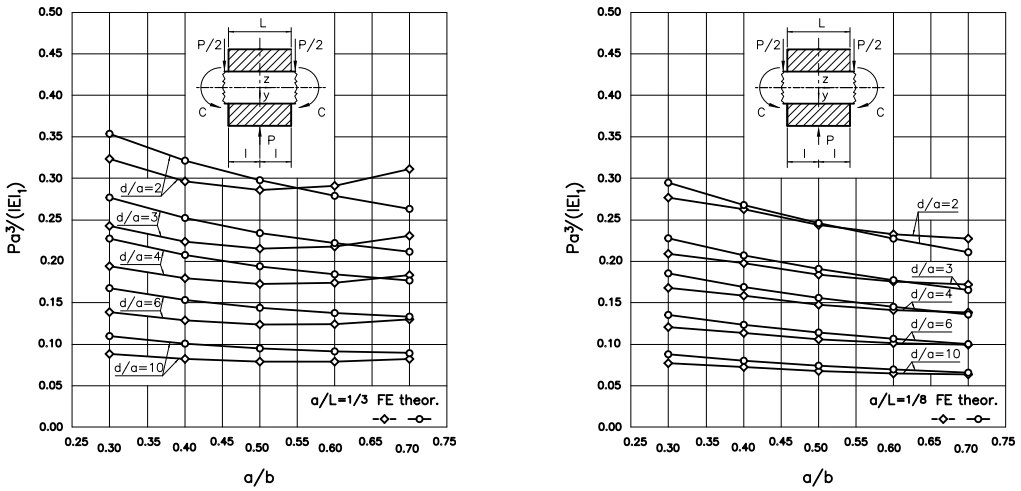

Figure 6. The value of the normalized detachment force $Pa^3/(IEI_1)$ versus a/b for $a/L = 1/3$ (left) and $a/L = 1/8$ (right), in the situation of incipient shaft-hub detachment, for $\nu = 0.3$.

7.1. ***Comparison between analytical and FE forecasts for the loading of Figure 1(a).*** For the non axisymmetric press-fit loading constituted by three radial forces, Figure 1(a), a suitable expression of the normalized force describing the detachment initiation derives from the analytical solution (5) of the ODE (2) within the respect of the boundary conditions (7). The analytical solution suggests that a proper normalized detachment force is $Pa^3/(IEI_1)$, where P represents the central load, a denotes the shaft radius, I is the diametric interference, E is the Young's modulus, and I_1 is the shaft moment of inertia. The detachment initiation force $Pa^3/(IEI_1)$ depends upon the three aspect ratios $a/b = \alpha$, d/a, a/L. The ranges explored with FE in Figure 6 for the three aspect ratios are $2 \le d/a \le 10$, $0.3 \le \alpha \le 0.7$, $1/8 \le a/L \le 1/3$. To limit the computational effort, only the two extreme values $1/3$ and $1/8$ of the variable a/L have been considered. The corresponding analytical and FE forecasts are presented in Figure 6, in which the abscissa variable is $a/b = \alpha$, the family of curves refers to five a/d values, and the ordinate variable is the normalized detachment force $Pa^3/(IEI_1)$.

The agreement between analytical and FE forecasts is on the whole acceptable, especially for $a/L = 1/8$, a coupling, this, whose geometry is better identifiable in terms of a beam.

In the following, the FE normalized detachment force $Pa^3/(IEI_1)$ of Figure 4 referring to $a/L = 1/8$ and to $d/a = 10$ is compared to the FE normalized detachment couple $Ca^2/(IEI_1)$ of Figure 5 of [Strozzi et al. 2016], also referring to $a/L = 1/8$. In fact, according Figure 4, the shaft extremity is loaded by a force $P/2$ acting at a distance d from the shaft section aligned with the hub lateral walls. For high values of d/a, the deforming effect of the bending couple $Pd/2$ acting on the shaft section aligned with the hub lateral walls is deemed to prevail over that of the shear force $P/2$. Consequently, $Ca^2/(IEI_1) = Pda^2/2/(IEI_1) = 5Pa^3/(IEI_1)$. In conclusion, the normalized couple of Figure 5 of [Strozzi et al. 2016] evaluated for $a/L = 1/8$, is expected to be about five times the normalized force of Figure 6, right, computed for $a/L = 1/8$ and for $d/a = 10$. For $a/b = 0.5$, the above ratio extracted from the FE forecasts of the two above diagrams is about 6, thus confirming the validity of the FE study.

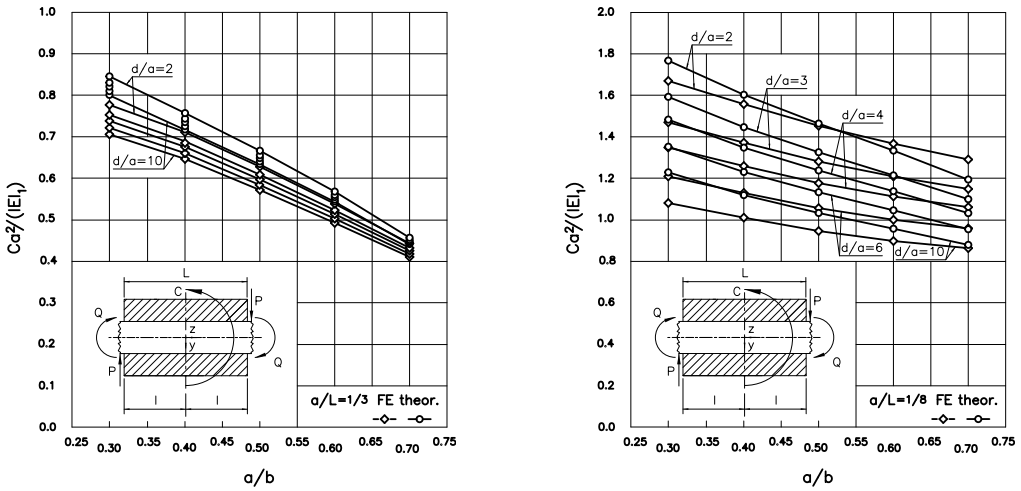

Figure 7. The value of the normalized detachment couple $Ca^2/(IEI_1)$ versus a/b for $a/L = 1/3$ (left) and $a/L = 1/8$ (right), in the situation of incipient shaft-hub detachment, for $\nu = 0.3$.

7.2. ***Comparison between analytical and FE forecasts for the loading of Figure 1(b).*** In the case of the loading of Figure 1(b), constituted by the couple C and by two equilibrating radial forces, a suitable normalized parameter that describes the press-fit incipient detachment is $Ca^2/(IEI_1)$. The detachment initiation couple $Ca^2/(IEI_1)$ depends upon the three aspect ratios $a/b = \alpha$, d/a, a/L. The ranges explored with FE for the three aspect ratios in Figure 7 coincide with those adopted for Figure 6. The agreement between analytical and FE forecasts is on the whole acceptable.

For $a/L = 1/3$, both the analytical and the FE curves referring to $d/a = 2, 3, 4, 6, 10$ are very similar. To avoid confusion in the diagram of Figure 5, only the analytical curves referring to the extremal d/a values 2 and 10 have been drawn. This essential independence of the normalized detachment couple of the parameter d/a suggests the rule of thumb according to which detachment occurs when $Ca^2/(IEI_1) \approx 0.4 \div 0.7$ for $2 \le d/a \le 10$ and $0.3 \le a/b \le 0.7$. A similar situation in which curves referring to various geometries are essentially superimposed occurs in Figure 5 of [Strozzi et al. 2016].

The reasonably favourable comparisons between analytical and FE predictions indicate that additional situations of incipient detachment may confidently be examined on the basis of the analytical predictions alone, without the need for a FE assessment. For instance, situations mentioned in the Introduction may analytically be examined in which, in a composite crankshaft, the shaft protrudes from only one side of the hub, whereas the remaining shaft extremity is aligned with one of the two hub lateral faces [Strozzi and Vaccari 2003].

8. Conclusions

A shaft-hub press fit subjected to two non-axisymmetric loading conditions has been examined, and the loading producing a situation of incipient detachment between the shaft and the hub has been determined. The first loading condition consists in a central radial load P sustained by the hub, equilibrated by

two lateral forces $P/2$ applied to the shaft at a distance d from the hub lateral walls. In the second loading condition a central couple C applied to the hub is equilibrated by two lateral loads withstood by the shaft at a distance d from the hub lateral walls, and exhibiting opposite directions. The shaft-hub contact has been modelled in terms of two elastic Timoshenko beams [Lanzoni and Radi 2016] connected by distributed elastic springs, whose constant has been analytically evaluated. Based upon this beam-like modelling, the loading inducing an undesired shaft-hub incipient detachment has been theoretically determined in term of the shaft-hub geometry, of the initial shaft-hub interference, and of the elastic constants. The analytical predictions of the incipient detachment loading have been compared to selected finite element forecasts, and the agreement has been found to be technically acceptable.

Acknowledgements

The authors are grateful to an anonymous reviewer for drawing their attention to the singular behaviour of the normalized Winkler constant for Poisson's ratios of about -0.9.

References

[Castillo and Barber 1997] J. Castillo and J. R. Barber, "Lateral contact of slender prismatic bodies", *Proc. Royal Soc. Lond. A Math. Phys. Engng. Sci.* **453** (1997), 2397–2412.

[Ciavarella et al. 1998] M. Ciavarella, D. A. Hills, and G. Monno, "The influence of rounded edges on indentation by a flat punch", *Proc. Inst. Mech. Engs., Part C: J. Mech. Eng. Sci.* **212**:4 (1998), 212–319.

[Croccolo et al. 2012] D. Croccolo, M. D. Agostinis, and N. Vincenzi, "Normalization of the stress concentrations at the rounded edges of a shaft-hub interference fit: extension to the case of a hollow shaft", *J. Strain Anal. Eng. Des.* **47** (2012), 131–139.

[Deseri and Owen 2003] L. Deseri and D. R. Owen, "Toward a field theory for elastic bodies undergoing disarrangements", *J. Elasticity* **70**:1-3 (2003), 197–236.

[Deseri and Owen 2010] L. Deseri and D. R. Owen, "Submacroscopically stable equilibria of elastic bodies undergoing disarrangements and dissipation", *Math. Mech. Solids* **15**:6 (2010), 611–638.

[Huang and Leissa 2007] C. S. Huang and A. W. Leissa, "Three-dimensional sharp corner displacement functions for bodies of revolution", *J. Appl. Mech.* (*ASME*) **74** (2007), 41–46.

[Lanzoni and Radi 2016] L. Lanzoni and E. Radi, "A loaded Timoshenko beam bonded to an elastic half plane", *Int. J. Solids Struct.* **92** (2016), 76–90.

[Love 1944] A. E. H. Love, *A treatise on the mathematical theory of elasticity*, vol. 1, Dover Publications, New York, 1944.

[Lundberg 1958] G. Lundberg, "Spannungen in pressverbänden bei belastung", *Die Kugellager Zeitschrift SKF* **3** (1958), 55–63.

[Marmorini et al. 2012] L. Marmorini, A. Baldini, E. Bertocchi, M. Giacopini, R. Rosi, and A. Strozzi, "On the loosening mechanism of a bush press-fitted in the small end of a connecting rod", *Proc. Ints. Mech. Eng. D: J. Automobile Eng.* **226**:3 (2012), 312–324.

[Radi et al. 2017] E. Radi, L. Lanzoni, A. Strozzi, and E. Bertocchi, "Shaft-hub press fit subjected to bending couples: analytical evaluation of the shaft-hub detachment couple", *Appl. Math. Model.* **50** (2017), 135–160.

[Smetana 2001] T. Smetana, *Untersuchungen zum Übertragungsverhalten biegebelasteter Kegel- und Zylinderpressverbindungen*, Shaker Verlag, 2001.

[Strozzi and Vaccari 2003] A. Strozzi and P. Vaccari, "On the press fit of a crankpin into a circular web in pressed-up crankshafts", *J. Strain Anal. Engng. Des.* **38** (2003), 189–199.

[Strozzi et al. 2011] A. Strozzi, A. Baldini, M. Giacopini, E. Bertocchi, and L. Bertocchi, "Normalization of the stress concentrations at the rounded edges of a shaft-hub interference fit", *J. Strain Anal. Eng. Des.* **46** (2011), 478–491.

[Strozzi et al. 2015] A. Strozzi, E. Bertocchi, A. Baldini, and M. Giacopini, "On the applicability of the Boussinesq influence function in modelling the frictionless elastic contact between a rectangular indenter with rounded edges and a half-plane", *Proc. Inst. Mech. Eng. C J. Mech. Engng. Sci.* **229** (2015), 987–1001.

[Strozzi et al. 2016] A. Strozzi, E. Bertocchi, A. Baldini, and S. Mantovani, "Normalization of the stress concentrations at the rounded edges of an interference fit between a solid shaft subjected to bending and a hub", *Mech. Based Des. Struct. Mach.* **44**:4 (2016), 405–425.

[Yosibash and Szabó 1995] Z. Yosibash and B. Szabó, "The solution of axisymmetric problems near singular points and computation of stress intensity factors", *Finite Elem. Anal. Des.* **19** (1995), 115–129.

Received 20 Nov 2017. Revised 26 Apr 2018. Accepted 30 Apr 2018.

ENRICO BERTOCCHI: enrico.bertocchi@unimore.it
DIEF-Dipartimento di Ingegneria Enzo Ferrari, Università di Modena e Reggio Emilia, Via Pietro Vivarelli 10, 41125 Modena, Italy

LUCA LANZONI: luca.lanzoni@unimo.it
DIEF-Dipartimento di Ingegneria Enzo Ferrari, Università di Modena e Reggio Emilia, Via Pietro Vivarelli 10, 41125 Modena, Italy

SARA MANTOVANI: sara.mantovani@unimore.it
DIEF-Dipartimento di Ingegneria Enzo Ferrari, Università di Modena e Reggio Emilia, Via Pietro Vivarelli 10, 41125 Modena, Italy

ENRICO RADI: enrico.radi@unimore.it
DISMI-Dipartimento di Scienze e Metodi dell'Ingegneria, Università di Modena e Reggio Emilia, Via Amendola, 2, 42122 Reggio Emilia, Italy

ANTONIO STROZZI: antonio.strozzi@unimore.it
DIEF-Dipartimento di Ingegneria Enzo Ferrari, Università di Modena e Reggio Emilia, Via Pietro Vivarelli 10, 41125 Modena, Italy

JOURNAL OF MECHANICS OF MATERIALS AND STRUCTURES

msp.org/jomms

Founded by Charles R. Steele and Marie-Louise Steele

See msp.org/jomms for submission guidelines.

JoMMS (ISSN 1559-3959) at Mathematical Sciences Publishers, 798 Evans Hall #6840, c/o University of California, Berkeley, CA 94720-3840, is published in 10 issues a year. The subscription price for 2018 is US $615/year for the electronic version, and $775/year (+$60, if shipping outside the US) for print and electronic. Subscriptions, requests for back issues, and changes of address should be sent to MSP.

JoMMS peer-review and production is managed by EditFLOW® from Mathematical Sciences Publishers.

PUBLISHED BY

mathematical sciences publishers

nonprofit scientific publishing

http://msp.org/

Journal of Mechanics of Materials and Structures

Volume 13, No. 3 May 2018